physics

IMPACT FACTOR 1.8

CITESCORE 3.1

Article

The Geometry of Qubit Decoherence: Linear Versus Nonlinear Dynamics in the Bloch Ball

Alan C. Maioli, Evaldo M. F. Curado, Jean-Pierre Gazeau and Tomoi Koide

Special Issue

A Themed Issue in Honor of Professor Viktor Dodonov—55 Years in Quantum Physics

Edited by

Prof. Dr. Andrei Klimov and Prof. Dr. Luis L. Sánchez-Soto

MDPI

https://doi.org/10.3390/physics8010008

physics

MDPI

Article

The Geometry of Qubit Decoherence: Linear Versus Nonlinear Dynamics in the Bloch Ball

Alan C. Maioli [1], Evaldo M. F. Curado [1,2], Jean-Pierre Gazeau [3,4,*] and Tomoi Koide [5]

[1] Centro Brasileiro de Pesquisas Físicas, Rio de Janeiro 22290-180, RJ, Brazil; alanmaioli@cbpf.br (A.C.M.); evaldo@cbpf.br (E.M.F.C.)
[2] National Institute of Science and Technology for Complex Systems, Rua Xavier Sigaud 150, Rio de Janeiro 22290-180, RJ, Brazil
[3] Laboratoire Astroparticule et Cosmologie, Université ParisCité, CNRS (Centre National de la Recherche Scientifique), 75013 Paris, France
[4] Faculty of Mathematics, University of Białystok, 15-245 Białystok, Poland
[5] Instituto de Física, Universidade Federal do Rio de Janeiro, C.P. 68528, Rio de Janeiro 21941-972, RJ, Brazil; tomoikoide@gmail.com
* Correspondence: gazeau@apc.in2p3.fr

Abstract

We present two complementary approaches to the Gorini–Kossakowski–Sudarshan–Lindblad equation for an open qubit. First, based on linearity, yields solutions illustrated by mixed-state trajectories in the Bloch ball, including non-random asymptotic fixed points and exceptional points. Second, exploiting the SU(2) symmetry, leads to a nonlinear dynamical system that separates angular dynamics from radial dissipation. This symmetry-based perspective presents a promising route toward generalization to open qudits.

Keywords: open quantum system; GLKS equation; qubit dynamical system; fixed points; exceptional points; Bloch ball; interacting spin qubit; SU(2) symmetry

1. Introduction

Studies in quantum physics have traditionally focused on systems isolated from their environment. However, with the recent developments in quantum computing [1] and quantum thermodynamics [2], the dynamics of open quantum systems have attracted growing interest. This line of research is also deeply connected to the measurement problem [3], an unresolved issue since the dawn of quantum mechanics, making it critical from both fundamental and applied perspectives [4–6].

The dynamics of such open quantum systems are to be derived from the microscopic unitary evolution of the total system (system plus environment), but this is generally quite complicated to perform. An axiomatic approach, therefore, becomes effective. Specifically, the dynamics of the system of interest are assumed linear and Markovian. Under these assumptions, if one imposes the requirement that the time evolution must preserve physical states, that is, a complete positiveness and trace-preservation (CPTP) map, it is known that the quantum master equation is the Gorini–Kossakowski–Sudarshan–Lindblad (GKSL) equation [2,7–9]. This equation unifies the treatment of the unitary evolution governed by the Hamiltonian of the system and the non-unitary dissipative processes described by GLKS jump operators, which represent the interaction with the environment. In particular, when applied to a single qubit (a two-level system), the fundamental unit of quantum information, its time evolution can be straightforwardly understood through a geometric

Received: 21 October 2025
Revised: 25 November 2025
Accepted: 3 December 2025
Published: 14 January 2026

picture using the Bloch vector [10]. In the representation based on Cartesian coordinates, this GKSL equation reduces to a tractable system of linear equations, and its solutions and properties have already been studied (see, for instance, Chapter 9 in Ref. [11]). In this paper, first, we revisit this system to analyze specific anisotropic cases, thereby clarifying how the interplay between Hamiltonian evolution and environmental dissipation gives rise to phenomena such as damped oscillations and the emergence of non-random, asymptotically stable fixed points within the mixed-state space.

This investigation highlights an essential feature for the design of robust qubits: by engineering the qubit–environment interaction, one can protect selected quantum states [12–15]. Furthermore, we explicitly identify the critical transition between oscillatory and monotonic decay regimes as an "exceptional point" in the spectrum of the Liouvillian superoperator. This result establishes a direct link between the geometric coalescence of state trajectories within the Bloch ball and the spectral degeneracies that characterize non-Hermitian quantum mechanics.

Further, in this paper, we develop an alternative descriptive framework for the same physical system by reformulating the dynamics in spherical coordinates, a representation that provides additional geometric clarity and facilitates the interpretation of anisotropic dissipation, fixed-point structure, and trajectory behavior within the Bloch ball. This coordinate transformation renders the equations of motion nonlinear, but it brings advantages that more than compensate for this complexity. First, it reveals a straightforward variable separation structure. Specifically, the radial variable, which is related to the change in the system's purity (and, thus, the informational entropy due to interaction with the environment), is naturally decoupled from the angular variables, which describe the orientation of the quantum state. This structure of variable separation is expected to hold universally, not only for two-level systems but also for general N-level systems. This provides an insightful theoretical framework for uniformly treating the dynamics of more complex quantum systems. Hence, we believe that our approach gives a new perspective on the geometric interpretation of the quantum information space. In addition, the unified geometric presentation presented here provides a pedagogically valuable perspective and is a practical tool for generalizations, as soon as it combines linear and nonlinear perspectives, revealing complementary physical insights. Our approach goes beyond standard linear solutions by deriving explicit nonlinear equations of motion for the qubit's orientation, which we identify as having a Ricatti-like structure [6]. Additionally, we obtain analytical trajectory invariants depicted as constants of motion for the dissipative path. To the best of our knowledge, such closed-form geometric constraints for anisotropic GKSL evolution have not been reported in the standard literature. The trajectory invariants provide a rigorous geometric description of the state's spiral toward the fixed point. This is followed by a discussion over the possible fixed points, which lie on the axes of the Bloch sphere representation.

The organization of the paper is as follows. In Section 2, we introduce the GKSL equation in the qubit case and proceed with its standard linear analysis in Cartesian coordinates. We then study the isotropic case and particular anisotropic situations. The examples are illustrated by showing trajectories in the Bloch ball. In Section 3, we proceed with an $SU(2)$ approach to the GLKS system which leads to the nonlinear dynamical system in spherical coordinates, of which the radial part shows the dissipative regime in a straightforward way. In Section 4, we perform a detailed study on the existence of fixed points and explore how they can be exploited to control the evolution of a qubit. In Section 5, we give insights about possible generalizations. Some details of computations made are given in Appendices A and B.

https://doi.org/10.3390/physics8010008

2. GKSL Equation

In this Section, we review the standard formulation of the GKSL equation for a single qubit. We employ the Bloch vector representation, which maps the density matrix to a vector in $\mathbb{R}^3$, and derive the linear system of differential equations that govern its dynamics. The starting point is the GKSL equation in the Schrödinger picture for a time deivative of a density matrix (i.e., quantum state) $\frac{\mathrm{d}\rho}{\mathrm{d}t}$, with the standard sign convention is:

$$\begin{aligned}\frac{\mathrm{d}\rho}{\mathrm{d}t} &= -\mathrm{i}\,[H,\rho] + \sum_k h_k \left[L_k \rho L_k^\dagger - \frac{1}{2}\left(\rho L_k^\dagger L_k + L_k^\dagger L_k \rho\right)\right] \\ &\equiv \mathcal{L}(\rho) = \mathcal{L}_{\mathrm{un}}(\rho) + \mathcal{L}_{\mathrm{diss}}(\rho)\,,\end{aligned} \tag{1}$$

where the symbol † denotes the Hermitian conjugate, H denotes the Hamiltonian, the L_k's along with the identity form an arbitrary basis of matrix operators, the coefficients h_k are non-negative constants with $k = 1,2,3 \equiv x,y,z$, and the reduced Planck constant is set to $\hbar = 1$. We also distinguish between the unitary Hamiltonian regime ($\mathcal{L}_{\mathrm{un}}$) and the dissipative regime ($\mathcal{L}_{\mathrm{diss}}$) in the action of the Lindblad operator $\mathcal{L}$. In the present two-dimensional case, a natural basis is the set compounded of the identity $\mathbb{1}_2$, the three Hermitian Pauli matrices σ_i, and the three anti-Hermitian matrices $\mathrm{i}\sigma_i$. This shows that only the subset $\{\mathbb{1}_2, \sigma_i\,,\ i = 1,2,3 \equiv x,y,z\}$ is necessary.

Let us write the density (i.e., non-negative Hermitian unit trace) operator as

$$\rho = \frac{1}{2}(\mathbb{1}_2 + a_1\sigma_1 + a_2\sigma_2 + a_3\sigma_3)\,, \quad \text{with} \quad \sqrt{a_1^2 + a_2^2 + a_3^2} \leq 1\,, \tag{2}$$

where $\vec{a}$ is the standard Bloch vector represented by a column matrix $\vec{a} = (a_1, a_2, a_3)^{\mathrm{T}}$, with the superscript "T" denoting the matrix transpose. Let us write the Hamiltonian in Pauli's matrices basis (considering the L_k as the Pauli matrices):

$$H = e_0\mathbb{1}_2 + e_1\sigma_1 + e_2\sigma_2 + e_3\sigma_3\,, \tag{3}$$

where e_i are constants.

Then GKSL Equation (1) results in the set of three equations (see Appendix B):

$$\begin{aligned}\dot{a}_1 &= 2(e_2a_3 - e_3a_2) - 2(h_2 + h_3)a_1\,, \\ \dot{a}_2 &= 2(e_3a_1 - e_1a_3) - 2(h_1 + h_3)a_2\,, \\ \dot{a}_3 &= 2(e_1a_2 - e_2a_1) - 2(h_1 + h_2)a_3\,,\end{aligned} \tag{4}$$

where the dot on top denotes the time derivative.

Thus, it can be rewritten in the following vector form characterizing a dynamical system:

$$\dot{\vec{a}} = 2\vec{e} \times \vec{a} - 2D_r \cdot \vec{a}\,, \tag{5}$$

$\vec{e} = (e_1, e_2, e_3)^{\mathrm{T}}$, while "$\times$" depicts the cross product. The matrix

$$D_r = \begin{pmatrix} h_2 + h_3 & 0 & 0 \\ 0 & h_1 + h_3 & 0 \\ 0 & 0 & h_1 + h_2 \end{pmatrix}, \tag{6}$$

contains the decay rates h_1, h_2, and h_3. Additionally, we write the cross product $\vec{e} \times \vec{a}$ as the product between the skew-symmetric matrix

$$e_\times = \begin{pmatrix} 0 & -e_3 & e_2 \\ e_3 & 0 & -e_1 \\ -e_2 & e_1 & 0 \end{pmatrix}, \tag{7}$$

and vector $\vec{a}$. One observes that the time derivative of the Bloch vector is equivalent to the matrix multiplication

$$\dot{\vec{a}} = T_d \cdot \vec{a}\,, \tag{8}$$

where

$$T_d = -2\begin{pmatrix} (h_2+h_3) & e_3 & -e_2 \\ -e_3 & (h_1+h_3) & e_1 \\ e_2 & -e_1 & (h_1+h_2) \end{pmatrix}. \tag{9}$$

2.1. Solutions to the System of Ode: Isotropic Case

In the case of time-independent dissipative factors h_k, Equation (8) can be solved by the known ansatz $\vec{a}(t) = \vec{v}\mathrm{e}^{\lambda t}$, where $\vec{v}$ is a constant vector. Then, Equation (8) reads

$$\lambda\vec{v}\mathrm{e}^{\lambda t} = T_d \cdot \vec{v}\,\mathrm{e}\lambda t\,, \tag{10}$$

where λ is a constant. The exponentials cancel out, leaving us with an eigenvalue problem. To simplify the formulation, we consider the isotropic case $h_1 = h_2 = h_3 = h$, which gives the following results for the eigenvalue problem:

$$\vec{v}_1 = (e_1, e_2, e_3)^{\mathrm{T}} = \vec{e}, \quad \lambda_1 = -4h\,, \tag{11}$$

$$\vec{v}_2 = \left(e_1e_2 + \mathrm{i}e_3\|\vec{e}\|\,,\ -(e_1^2+e_3^2),\ e_2e_3 - \mathrm{i}e_1\|\vec{e}\|\right)^{\mathrm{T}}, \quad \lambda_2 = -4h - 2\mathrm{i}\|\vec{e}\|\,, \tag{12}$$

$$\vec{v}_3 = \left(-e_1e_2 + \mathrm{i}e_3\|\vec{e}\|\,,\ (e_1^2+e_3^2),\ -e_2e_3 - \mathrm{i}e_1\|\vec{e}\|\right)^{\mathrm{T}}, \quad \lambda_3 = -4h + 2\mathrm{i}\|\vec{e}\|\,. \tag{13}$$

Then, we find the solution:

$$\vec{a}(t) = C_1\vec{e}\,\mathrm{e}^{-4ht} + C_2\vec{v}_2\mathrm{e}^{-4ht-2\mathrm{i}\|\vec{e}\|t} + C_3\vec{v}_3\mathrm{e}^{-4ht+2\mathrm{i}\|\vec{e}\|t}\,, \tag{14}$$

where the coefficients C_1, C_2, and C_3 are to be determined by an initial condition $\vec{a}(0)$.

2.2. Physical Illustrative Example

In this Section, we consider a spin-1/2 particle interacting with a magnetic field $\vec{B} = \omega_0\hat{z}$, where ω_0 is a constant. So, the Hamiltonian is $H = \omega_0\sigma_z$, which gives $\vec{e} = (0,0,\omega_0)^{\mathrm{T}}$. Setting initial condition $\vec{a}(0) = (1,0,0)^{\mathrm{T}}$, the solution is

$$\vec{a}(t) = \mathrm{e}^{-4ht}(\cos 2\omega_0 t,\ \sin 2\omega_0 t,\ 0)^{\mathrm{T}}\,, \tag{15}$$

and the trajectories are visualized in Figure 1. The second example is related to the initial condition $\vec{a}(0) = (1/\sqrt{2})(1,0,1)$, which yields the following solution:

$$\vec{a}(t) = \frac{\mathrm{e}^{-4ht}}{\sqrt{2}}(\cos 2\omega_0 t,\ \sin 2\omega_0 t,\ 1)^{\mathrm{T}}\,. \tag{16}$$

The time evolution of the state vector (16), as depicted by its trajectory on the Bloch sphere in Figure 1, reveals a precessional motion coupled with an inward spiral. This behavior is similar to a damped rotating system. Consequently, this representative case serves as an example for illustrating the interplay between unitary evolution, which manifests as rotation driven by the Hamiltonian (3) and non-unitary, dissipative evolution, which is responsible for the observed damping effect, as shown in Figure 2.

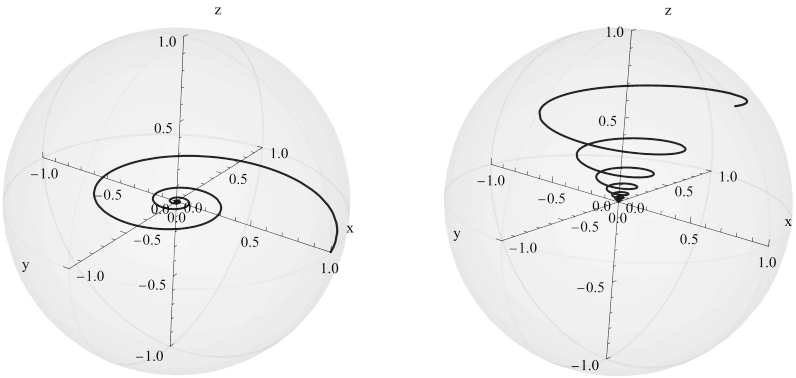

Figure 1. Trajectories of the quantum state given by Equations (15) and (16) related to the initial condition **(left)** $\vec{a}(0) = (1,0,0)^{\mathrm{T}}$ and **(right)** $\vec{a}(0) = (1/\sqrt{2})(1,0,1)^{\mathrm{T}}$, with the Hamiltonian $H = \omega_0\sigma_z$, where $\omega_0 = 10$, $h = 1$.

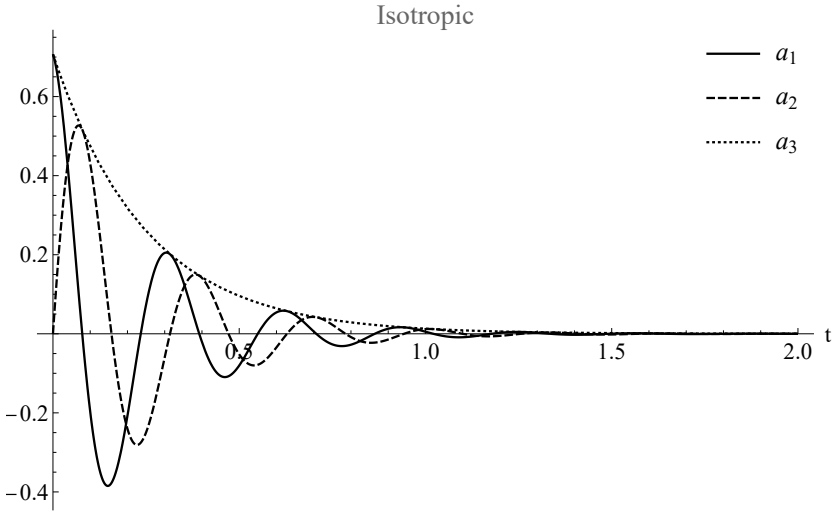

Figure 2. Time evolution of the components $a_i(t)$ of the example related to Equation (16), with the initial condition $\vec{a}(0) = (1/\sqrt{2})(1,0,1)$, and with environment isotropic interactions.

2.3. Anisotropic Case

Setting $h_1 = h$, and $h_2 = h_3 = 0$ and the Hamiltonian $H = \omega_0\sigma_z$ gives the following matrix T_d (9)

$$T_d = -2\begin{pmatrix} 0 & \omega_0 & 0 \\ -\omega_0 & h & 0 \\ 0 & 0 & h \end{pmatrix}. \tag{17}$$

It is convenient to introduce the parameter $\beta = h/2\omega_0$ and its pseudo-Lorentz companion $\widetilde{\gamma} = 1/\sqrt{\beta^2 - 1}$.

The eigenvectors and eigenvalues of T_d (17) then reads

$$\vec{v}_4 = (0,0,1)^{\mathrm{T}}, \qquad \lambda_4 = -2h, \tag{18}$$

$$\vec{v}_5 = (\beta - 1/\widetilde{\gamma},\ 1,\ 0)^{\mathrm{T}}, \qquad \lambda_5 = 2\omega_0(-\beta - 1/\widetilde{\gamma}), \tag{19}$$

$$\vec{v}_6 = (\beta + 1/\widetilde{\gamma},\ 1,\ 0)^{\mathrm{T}}, \qquad \lambda_6 = 2\omega_0(-\beta + 1/\widetilde{\gamma}). \tag{20}$$

One obtains

$$\vec{a}(t) = C_4\vec{v}_4 e^{-2ht} + C_5\vec{v}_5 e^{-ht-2\frac{\omega_0}{\widetilde{\gamma}}t} + C_6\vec{v}_6 e^{-ht+2\frac{\omega_0}{\widetilde{\gamma}}t}. \tag{21}$$

Supposing an initial condition $\vec{a}(0) = (1,\ 0,\ 0)^{\mathrm{T}}$, one finds the solution

$$\vec{a}(t) = \left(\mathrm{e}^{-ht}\left[\cosh\left(2\frac{\omega_0}{\widetilde{\gamma}}t\right) + \widetilde{\gamma}\beta\sinh\left(2\frac{\omega_0}{\widetilde{\gamma}}t\right)\right],\ \widetilde{\gamma}\mathrm{e}^{-ht}\sinh\left(2\frac{\omega_0}{\widetilde{\gamma}}t\right),\ 0\right)^{\mathrm{T}}. \tag{22}$$

For different values of β, the system enters different dissipative regimes, such as oscillatory regime $\beta < 1$, damped regime $\beta > 1$, and critical regime $\beta = 1$. These differences are visualized in Figure 3.

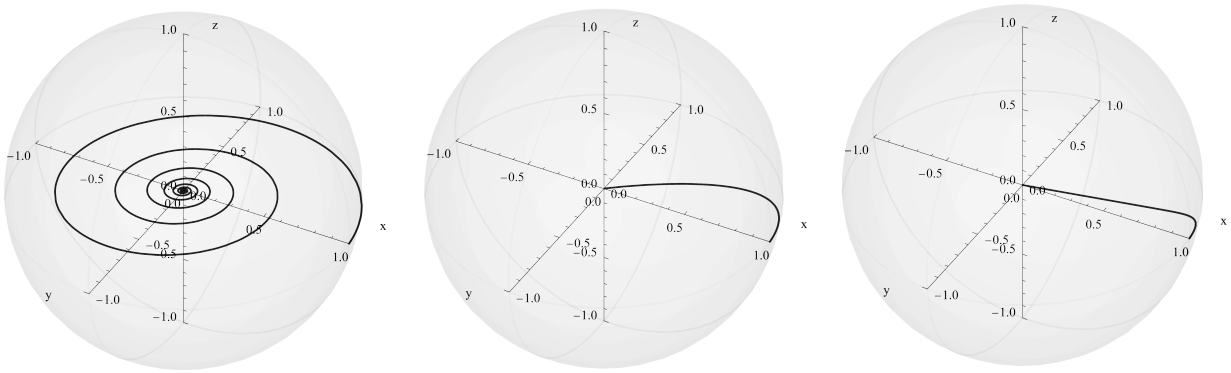

Figure 3. Trajectory of the system in the Bloch ball for the three regimes: (**left**) oscillation/subcritical ($\beta = h/2\omega_0 < 1$) with the decay rate $h = 2$, (**middle**) critical ($\beta = 1$) with $h = 20$, and (**right**) supercritical ($\beta > 1$) with $h = 50$. The contribution of the Hamiltonian is set to $\omega_0 = 10$ and the initial condition is $\vec{a}(0) = (1, 0, 0)^{\mathrm{T}}$.

The subcritical damping is achieved by choosing $\beta < 1$, where the qubit behaves as an oscillatory system with damping. By introducing the Lorentzian companion $\gamma = 1/\sqrt{1-\beta^2}$, Equation (22) reads

$$\vec{a}(t) = \left(\mathrm{e}^{-ht}\left[\cos\left(2\frac{\omega_0}{\gamma}t\right) + \beta\gamma\sin\left(2\frac{\omega_0}{\gamma}t\right)\right],\ \gamma\mathrm{e}^{-ht}\sin\left(2\frac{\omega_0}{\gamma}t\right),\ 0\right)^{\mathrm{T}}, \tag{23}$$

and it is possible to determine the period of the oscillation $\tau = \pi\gamma/\omega_0$.

The supercritical regime is found for the values $\beta > 1$. In this case, solution of $\vec{a}(t)$ (22) relies on the hyperbolic trigonometric function, which can be rewritten as exponentials. Thus, for sufficiently long times, one may factor out the dominant contribution $\mathrm{e}^{(-h+2\omega_0/\widetilde{\gamma})t}$, which naturally leads to the definition of a characteristic decay time

$$\tau_d = \frac{(\beta + \sqrt{\beta^2 - 1})}{2\omega_0}. \tag{24}$$

For $t \gg \tau_d$, the system behave as $\|\vec{a}(t)\| \propto \mathrm{e}^{-t/\tau_d}$; see Appendix A for details.

The last regime appears at the critical point $\beta = 1$, i.e., $h = 2\omega_0$, which has the solution

$$\vec{a}(t) = \mathrm{e}^{-2\omega_0 t}(1 + 2\omega_0 t,\ 2\omega_0 t,\ 0)^{\mathrm{T}}. \tag{25}$$

This system exhibits a behavior quite similar to that of a classical damped harmonic oscillator, in which the most rapid decay occurs in the critically damped regime. This feature is well visible in Figure 4 (and for each Bloch component in Figure 5). The analogy stems from the competition between the unitary Hamiltonian dynamics and the dissipative influence of the environment: the former induces rotations generated by the interaction along the z-axis through the action of $\sigma_3 = \sigma_z$, whereas the latter produces damping along the x-axis via the action of $\sigma_1 = \sigma_x$. For completeness, Figure 5 displays the time

evolution of the individual Bloch components for the anisotropic cases, thereby illustrating the different decay regimes.

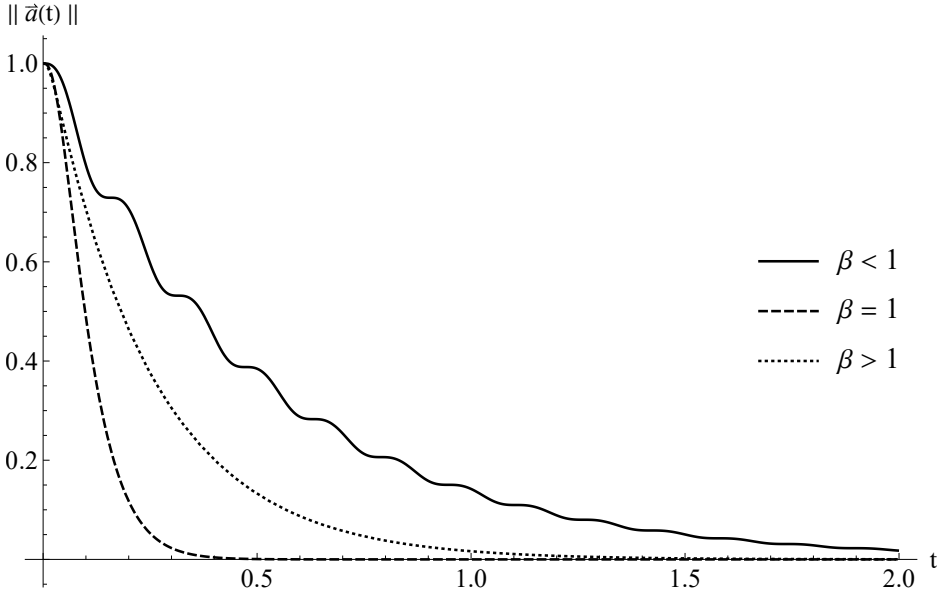

Figure 4. Decay comparison of the examples from Figure 3, for the three regimes: oscillation/subcritical $\beta < 1$, critical $\beta = 1$, and supercritical $\beta > 1$. The system related to the critical case decays faster than the two others.

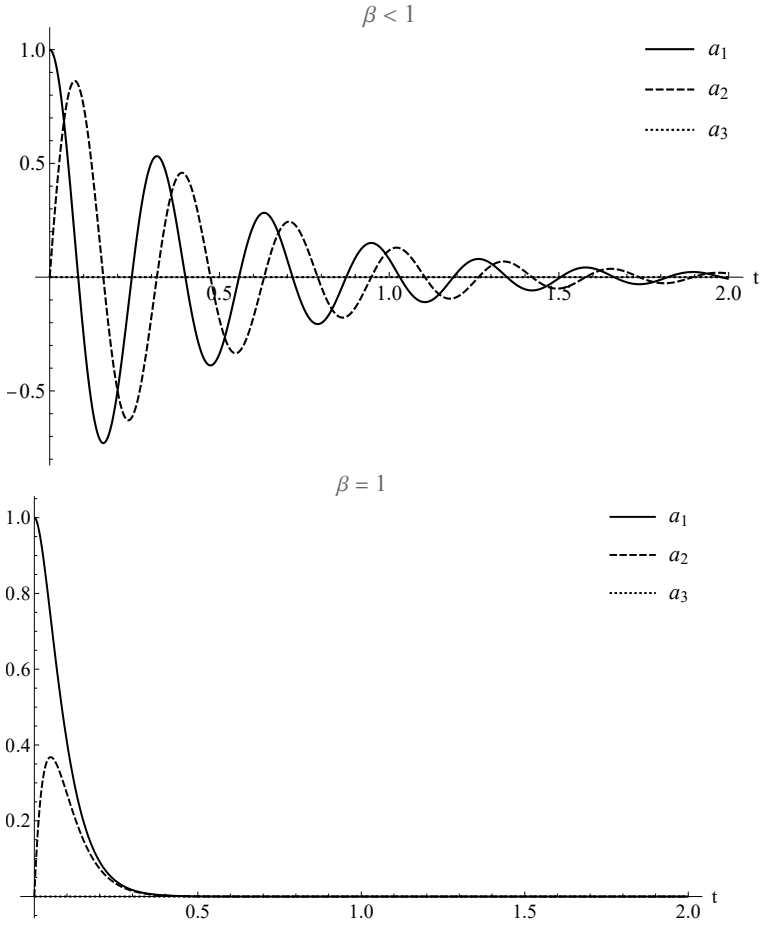

Figure 5. *Cont.*

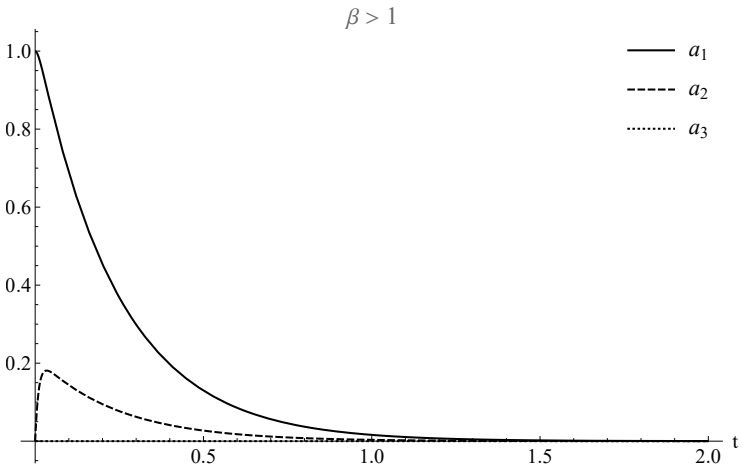

Figure 5. Time evolution of the components $a_i(t)$ of the $\vec{a}(t)$ associated with the Pauli matrices σ_i, $i = 1, 2$ and 3, for the (**upper**) subcritical, (**middle**) critical, and (**lower**) supercritical regimes.

2.4. One Direction

Here, we explore the behavior of the system when both the Hamiltonian and decay rate are related to σ_z. Then $H = \omega_0\sigma_z$, $h_1 = h_2 = 0$, while $h_3 = h$, and

$$T_d = -2\begin{pmatrix} h & \omega_0 & 0 \\ -\omega_0 & h & 0 \\ 0 & 0 & 0 \end{pmatrix}. \tag{26}$$

Therefore, the action of matrix T_d (26) over the Bloch vector $\vec{a}$ only affects the σ_x and σ_y directions, leaving the σ_z unchanged. Along these lines, a state that is initially $\vec{a}(0) = (0, 0, 1)^{\mathrm{T}}$ does not change over time, which can be represented as a fixed point of the GKSL equation.

On the other hand, a state that has σ_x or σ_y components rotates and decays; for example, the state $\vec{a}(0) = (1, 0, 1)^{\mathrm{T}}/\sqrt{2}$ evolves according to

$$\vec{a}(t) = \frac{1}{\sqrt{2}}\left(\mathrm{e}^{-2ht}\cos 2\omega_0 t\ ,\ \mathrm{e}^{-2ht}\sin 2\omega_0 t\ ,\ 1\right)^{\mathrm{T}}, \tag{27}$$

and is visualized in Figure 6, while the σ_z component remains constant.

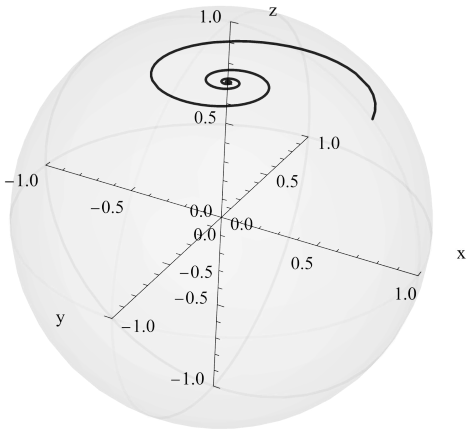

Figure 6. Trajectory of the state (27), with $\omega_0 = 5$ and $h = 1$, the initial condition $\vec{a}(0) = (1/\sqrt{2})(1, 0, 1)^{\mathrm{T}}$ and the σ_z direction unchange over time.

This example shows that a state with components only along the σ_z direction is a fixed point of the evolution, and it can be seen in the solution before setting the initial condition

$$\vec{a}(t) = \left(-ic_2 e^{-2t(h+i\omega_0)} + ic_3 e^{-2t(h-i\omega_0)},\ c_2 e^{-2t(h+i\omega_0)} + c_3 e^{-2t(h-i\omega_0)},\ c_1\right)^{\mathrm{T}}, \tag{28}$$

and setting $c_2 = c_3 = 0$. More generally, each point in the z-axis acts as an attractor for the dynamics in the xy-plane. In other words, any initial state decoheres in the xy-plane while preserving its z-component, eventually converging to a final state on the z-axis. This line of fixed points represents the set of stable equilibrium states for the qubit under this specific Hamiltonian and dissipative channel. This phenomenon illustrates a strategy for enhancing qubit stability by engineering a dominant environmental interaction to create a (almost) decoherence-free subspace; the computational basis states (i.e, $|\uparrow\rangle$ and $|\downarrow\rangle$ as eigenstates of σ_z, with the arrows ponting the spin direction (up or down)) become robust states that act like a pointer state.

2.5. Exceptional Points: Discussion

In a broader context, the exceptional points (EPs) [16,17] are non-Hermitian degeneracies at which both eigenvalues and their corresponding eigenvectors coalesce, leading to a breakdown of the conventional Hermitian spectral theory. In quantum systems, EPs emerge when dissipation or gain introduces non-conservativity, rendering the effective Hamiltonian non-Hermitian. This results in a characteristic spectral topology, where eigenvalues exhibit square-root branch point behavior. For a single qubit subject to engineered loss, such as in superconducting circuits or optical platforms, the Hamiltonian can be tailored to realize an EP by balancing coherent coupling and decay rates. In this regime, the qubit exhibits a non-trivial evolution marked by spontaneous symmetry breaking, mode non-orthogonality, and enhanced sensitivity to perturbations. Importantly, recent experimental realizations have demonstrated quantum state tomography across EPs [18], revealing distinctive features such as the coalescence of decay rates at the EP, the transition between underdamped and overdamped dynamics, and signatures of parity-time PT-symmetry breaking in the relaxation pathways of the qubit.

In the anisotropic single-qubit model presented in this Section, the effective Bloch evolution is generated by the non-Hermitian matrix T_d (17). The eigenvalues of T_d determine three dynamical regimes (subcritical, critical, and supercritical), analogous to a damped harmonic oscillator. At the critical point ($\beta = 1$), two eigenvalues and eigenvectors coalesce, indicating a Liouvillian exceptional point. In other words, a non-Hermitian degeneracy occurs in the Liouvillian superoperator of the open quantum system. The dynamics near this point are qualitatively distinct, with the fastest decay consistent with known non-Hermitian degeneracies.

3. SU(2) Symmetry Content of GLKS Dynamics

In this Section, an approach to the GLKS system based on the underlying SU(2) symmetry and related tools are adopted. Although we (artificially) leave linearity out of the system, we unveil an instructive separation between the angular regime, which involves the whole Lindblad operator $\mathcal{L}$ and the radial regime rule, which is explicitly ruled by $\mathcal{L}_{\mathrm{diss}}$ only. More precisely, the SU(2) symmetry approach, specifically, the left coset SU(2)/U(1) symmetry, decouples the dynamics of the system. This approach provides a link between the change in the state's purity, the decay rates, and the evolution of its orientation and on the Bloch sphere as a nonlinear dynamical system.

3.1. $SU(2)$ Content of Density Matrix

An arbitrary density operator in $\mathbb{C}^2$ has the following spectral decomposition:

$$\rho = p_1 \mathrm{P}_{\mathbf{u}_1} + p_2 \mathrm{P}_{\mathbf{u}_2}\,, \quad p_1 + p_2 = 1\,, \tag{29}$$

where $p_i \in [0,1]$ has a classical probability sense and $\mathrm{P}_{\mathbf{u}_i} = |\mathbf{u}_i\rangle\langle\mathbf{u}_i|$ is an orthogonal projector (pure states) on eigendirections $\mathbf{u}_i$, $i = 1,2$. No degeneracy and $p_1 > p_2 > 0$ (generic situation) are supposed here. By introducing the element of $U(\theta,\phi) \in \mathrm{SU}(2)/\mathrm{U}(1)$, which diagonalizes ρ, the latter can be written as

$$\rho \equiv \rho_{r,\theta,\phi} = \frac{1}{2}\Big(\mathbb{1}_2 + rU(\theta,\phi)\sigma_3 U^\dagger(\theta,\phi)\Big) \equiv \frac{1}{2}\big(\mathbb{1}_2 + r\sigma_{\theta,\phi}\big)\,, \tag{30}$$

with

$$U(\theta,\phi) := \begin{pmatrix} \cos\frac{\theta}{2} & -\sin\frac{\theta}{2}\,\mathrm{e}^{-\mathrm{i}\phi} \\ \sin\frac{\theta}{2}\,\mathrm{e}^{\mathrm{i}\phi} & \cos\frac{\theta}{2} \end{pmatrix}, \quad \theta \in [0,\pi]\,, \quad \phi \in [0,2\pi)\,, \tag{31}$$

and $r = 2p_1 - 1 \in [0,1]$ is the normalized excess of p_1 above the uniform baseline. The matrix $\sigma_{\theta,\phi}$ in Equation (30) is a traceless involution (involution means its square is the identity) in $\mathrm{SU}(2)$:

$$\sigma_{\theta,\phi} = U(\theta,\phi)\sigma_3 U^\dagger(\theta,\phi) = \begin{pmatrix} \cos\theta & \sin\theta\,\mathrm{e}^{-\mathrm{i}\phi} \\ \sin\theta\,\mathrm{e}^{\mathrm{i}\phi} & -\cos\theta \end{pmatrix}, \quad \sigma_{\theta,\phi} = \sigma^\dagger_{\theta,\phi}\,, \quad \sigma^2_{\theta,\phi} = \mathbb{1}_2\,. \tag{32}$$

We check that $(\theta,\phi) \mapsto U(\theta,\phi)$ is a representation of the half-circle,

$$U(\theta,\phi)U(\theta',\phi) = U(\theta+\theta',\phi)\,. \tag{33}$$

This property is consistent with the feature that $U(\theta,\phi)$ is an element of the left coset $\mathrm{SU}(2)/\mathrm{U}(1)$, since any right $\mathrm{U}(1)$ factor $\begin{pmatrix} \mathrm{e}^{\mathrm{i}\omega} & 0 \\ 0 & \mathrm{e}^{-\mathrm{i}\omega} \end{pmatrix}$ of $U(\theta,\phi)$ in Equation (30) is transparent, due to the feature it commutes with σ_3. Its column vectors

$$\mathbf{u}_1 = \begin{pmatrix} \cos\frac{\theta}{2} \\ \sin\frac{\theta}{2}\mathrm{e}^{\mathrm{i}\phi} \end{pmatrix}, \quad \mathbf{u}_2 = \begin{pmatrix} -\sin\frac{\theta}{2}\mathrm{e}^{-\mathrm{i}\phi} \\ \cos\frac{\theta}{2} \end{pmatrix}, \tag{34}$$

which form an orthonormal basis for $\mathbb{C}^2$, are precisely the normalized eigenvectors of ρ, consistent with the notation in Equation (29). Moreover, they can be viewed as spin one-half coherent states $|\theta,\phi\rangle$, defined in terms of spherical coordinates (θ,ϕ) as the quantum counterpart of the classical state $\hat{\mathbf{n}}(\theta,\phi)$ in the (Bloch) sphere $\mathbb{S}^2$ by

$$\begin{aligned} \mathbf{u}_1 &= \begin{pmatrix} \cos\frac{\theta}{2} \\ \sin\frac{\theta}{2}\mathrm{e}^{\mathrm{i}\phi} \end{pmatrix} \equiv |\theta,\phi\rangle = \Big(\cos\frac{\theta}{2}\,|\uparrow\rangle + \mathrm{e}^{\mathrm{i}\phi}\sin\frac{\theta}{2}\,|\downarrow\rangle\Big) \\ &= \begin{pmatrix} \cos\frac{\theta}{2} & -\sin\frac{\theta}{2}\mathrm{e}^{-\mathrm{i}\phi} \\ \sin\frac{\theta}{2}\mathrm{e}^{\mathrm{i}\phi} & \cos\frac{\theta}{2} \end{pmatrix}\begin{pmatrix} 1 \\ 0 \end{pmatrix} = U(\theta,\phi)|\uparrow\rangle \equiv D^{\frac{1}{2}}\Big(\xi^{-1}_{\hat{\mathbf{n}}}\Big)|\uparrow\rangle\,. \end{aligned} \tag{35}$$

Here, $\xi_{\hat{\mathbf{n}}}$ corresponds, through the homomorphism $\mathrm{SO}(3) \mapsto \mathrm{SU}(2)$, to the specific rotation $\mathcal{R}_{\hat{\mathbf{n}}}$ in the Bloch sphere, which maps the unit vector pointing to the north pole, $\hat{\boldsymbol{k}} = (0,0,1)$, to $\hat{\mathbf{n}}$. The operator $D^{\frac{1}{2}}\Big(\xi^{-1}_{\hat{\mathbf{n}}}\Big)$ represents the element $\xi^{-1}_{\hat{\mathbf{n}}}$ of $\mathrm{SU}(2)$ in its complex two-dimensional unitary irreducible representation. Thus, the spectral decomposition (29) of $\rho_{r,\theta,\phi}$ is expressed in terms of the two orthogonal spin coherent states :

$$\rho_{r,\theta,\phi} = \frac{1+r}{2}|\theta,\phi\rangle\langle\theta,\phi| + \frac{1-r}{2}|\theta+\pi,\phi\rangle\langle\theta+\pi,\phi|\,. \tag{36}$$

We reiterate here some fundamental properties of these coherent states :

$$\langle\theta,\phi|\theta,\phi\rangle = 1\,, \quad \int_{\mathbb{S}^2} \frac{\mathrm{d}\mathbf{u}}{4\pi}\,|\theta,\phi\rangle\langle\theta,\phi| = \mathbb{1}_2\,, \quad \mathrm{d}\mathbf{u} = \sin\theta\,\mathrm{d}\theta\,\mathrm{d}\phi\,. \tag{37}$$

Note the extreme cases $r = 1$ (pure state equivalent to spin coherent state) and $r = 0$ (totally random state):

$$\rho_{1,\theta,\phi} = |\theta,\phi\rangle\langle\theta,\phi|\,, \quad \rho_0 = \frac{1}{2}\mathbb{1}_2\,. \tag{38}$$

3.2. GLKS System in Terms of Parameters (R,θ,ϕ)

3.2.1. Radial Dissipation

Let us now formulate the GLKS system (1) in functions of the Bloch ball parameters (r,θ,ϕ). First, by using the expression (30), one obtains for the time derivative of $\rho_{r,\theta,\phi}$

$$\frac{\mathrm{d}\rho_{r,\theta,\phi}}{\mathrm{d}t} = \frac{\dot{r}}{2}\,\sigma_{\theta,\phi} + \frac{r}{2}\,\frac{\mathrm{d}\sigma_{\theta,\phi}}{\mathrm{d}t}\,. \tag{39}$$

Now, from Equation (32) and the identities $UU^\dagger = \mathbb{1}_2 = U^\dagger U \Rightarrow \dot{U}U^\dagger = -U\dot{U}^\dagger$, one finds

$$\frac{\mathrm{d}\sigma_{\theta,\phi}}{\mathrm{d}t} = \dot{U}\sigma_3 U^\dagger + U\sigma_3\dot{U}^\dagger = \left[\dot{U}U^\dagger, \sigma_{\theta,\phi}\right]. \tag{40}$$

Thus, the Lindblad equation takes the form

$$\frac{\dot{r}}{2}\,\sigma_{\theta,\phi} + \frac{r}{2}\left[\dot{U}U^\dagger, \sigma_{\theta,\phi}\right] = -\mathrm{i}\frac{r}{2}\left[H, \sigma_{\theta,\phi}\right] + \frac{r}{2}\sum_{k=1}^{3} h_k\left(\sigma_k\,\sigma_{\theta,\phi}\,\sigma_k - \sigma_{\theta,\phi}\right). \tag{41}$$

Using $\sigma_{\theta,\phi}^2 = \mathbb{1}_2$, one finds

$$\frac{\dot{r}}{r}\mathbb{1}_2 = \left[\sigma_{\theta,\phi}, \dot{U}U^\dagger + \mathrm{i}H\right]\sigma_{\theta,\phi} + \sum_{k=1}^{3} h_k\left[\left(\sigma_k\sigma_{\theta,\phi}\right)^2 - \mathbb{1}_2\right]. \tag{42}$$

Taking the trace (Tr) of Equation (42) and using $\mathrm{Tr}\left(\left[\sigma_{\theta,\phi}, A\right]\sigma_{\theta,\phi}\right) = \mathrm{Tr}\left(\sigma_{\theta,\phi}A\sigma_{\theta,\phi} - A\right) = 0$ for all $A \in \mathrm{M}(2,\mathbb{R})$, one finds the following equation:

$$\begin{aligned}\frac{\dot{r}}{r} &= \frac{1}{2}\left(\sum_{k=1}^{3} h_k\left(\mathrm{Tr}\left(\sigma_k\sigma_{\theta,\phi}\right)^2 - 2\right)\right)\\ &= -2\left[h_1(1-\sin^2\theta\cos^2\phi) + h_2(1-\sin^2\theta\sin^2\phi) + h_3\sin^2\theta\right].\end{aligned} \tag{43}$$

Let us note that there is no explicit dependence of the Hamiltonian. The action of the latter is implicit only through the time dependence of the angles θ and ϕ. Since the decay rates h_k are non-negative, the entire expression on the right-hand side is always less than or equal to zero. Henceforth, Equation (43) is a fundamental result that directly connects the change in the state's purity to the decay rates. The parameter r is a measure of the state's purity, where $r = 1$ is a pure state and $r = 0$ is a maximally mixed state. This proves that $\dot{r} \leq 0$, meaning the purity of the state can only decrease or remain constant over time. The finding that $\dot{r} \leq 0$ confirms the principle of dissipation, as the system loses coherence to its environment. This interpretation is confirmed with the increase in the von Neumann entropy:

$$S_\rho := -\mathrm{Tr}(\rho\,\ln\rho) = -\frac{1+r}{2}\ln\frac{1+r}{2} - \frac{1-r}{2}\ln\frac{1-r}{2}\,, \quad \dot{S_\rho} = -\frac{\dot{r}}{2}\ln\frac{1+r}{1-r} \geq 0\,. \tag{44}$$

3.2.2. Angular Dynamical System

Let us now decouple the angular variables' motions from the radial one, starting from Equation (42) and using Equation (43). By introducing the two traceless matrix expressions one finds

$$M(\theta,\phi) = \sum_{k=1}^{3} h_k \left[\left(\sigma_k \sigma_{\theta,\phi}\right)^2 - \frac{1}{2}\left(\mathrm{Tr}\left(\sigma_k \sigma_{\theta,\phi}\right)^2\right) \mathbb{1}_2 \right], \quad \mathrm{Tr}\, M(\theta,\phi) = 0\,, \tag{45}$$

$$N(\theta,\phi) = -\mathrm{i}\left[H, \sigma_{\theta,\phi}\right] \sigma_{\theta,\phi} + M(\theta,\phi) \tag{46}$$

and then obtains the matrix dynamical system for angular variables (θ,ϕ):

$$\left[\dot{U}U^\dagger, \sigma_{\theta,\phi}\right] \sigma_{\theta,\phi} = N(\theta,\phi)\,. \tag{47}$$

We now make explicit $\dot{U}$ and $\dot{U}U^\dagger \equiv \dot{X}$ in terms of $\dot{\phi}$ and $\dot{\theta}$ from the matrix (31). Here, X is the anti-Hermitian "logarithm" of U:

$$U = \mathrm{e}^X\,, \quad X \in \mathfrak{su}(2)\,, \quad \dot{U}U^\dagger = \dot{X}\,. \tag{48}$$

$$\begin{aligned} \dot{U} &= \mathrm{i}\dot{\phi} \sin\frac{\theta}{2} \begin{pmatrix} 0 & \mathrm{e}^{-\mathrm{i}\phi} \\ \mathrm{e}^{\mathrm{i}\phi} & 0 \end{pmatrix} + \frac{\dot{\theta}}{2} \begin{pmatrix} -\sin\frac{\theta}{2} & -\mathrm{e}^{-\mathrm{i}\phi}\cos\frac{\theta}{2} \\ \mathrm{e}^{\mathrm{i}\phi}\cos\frac{\theta}{2} & -\sin\frac{\theta}{2} \end{pmatrix} \\ &= \mathrm{i}\dot{\phi} \sin\frac{\theta}{2}\, \mathrm{n}(\phi) + \frac{\dot{\theta}}{2}\, U(\theta+\pi,\phi)\,, \end{aligned} \tag{49}$$

where we introduce the Hermitian involution

$$\mathrm{n}(\phi) = \begin{pmatrix} 0 & \mathrm{e}^{-\mathrm{i}\phi} \\ \mathrm{e}^{\mathrm{i}\phi} & 0 \end{pmatrix}, \quad \mathrm{n}^\dagger(\phi) = \mathrm{n}(\phi)\,, \quad \mathrm{n}^2(\phi) = \mathbb{1}_2\,. \tag{50}$$

Hence, one finds the following for Equation (49):

$$\begin{aligned} \dot{U}U^\dagger = \dot{X} &= \mathrm{i}\dot{\phi} \sin\frac{\theta}{2} \begin{pmatrix} -\sin\frac{\theta}{2} & \cos\frac{\theta}{2}\mathrm{e}^{-\mathrm{i}\phi} \\ \cos\frac{\theta}{2}\mathrm{e}^{\mathrm{i}\phi} & \sin\frac{\theta}{2} \end{pmatrix} + \frac{\dot{\theta}}{2} \begin{pmatrix} 0 & -\mathrm{e}^{-\mathrm{i}\phi} \\ \mathrm{e}^{\mathrm{i}\phi} & 0 \end{pmatrix} \\ &= \mathrm{i}\dot{\phi} \sin\frac{\theta}{2}\, \mathrm{F}(\theta,\phi) + \frac{\dot{\theta}}{2}\, \mathrm{s}(\phi)\,, \end{aligned} \tag{51}$$

where the traceless involution matrix

$$\mathrm{F}(\theta,\phi) = \begin{pmatrix} -\sin\frac{\theta}{2} & \cos\frac{\theta}{2}\mathrm{e}^{-\mathrm{i}\phi} \\ \cos\frac{\theta}{2}\mathrm{e}^{\mathrm{i}\phi} & \sin\frac{\theta}{2} \end{pmatrix}, \quad \mathrm{F}^2(\theta,\phi) = \mathbb{1}_2\,, \quad \det \mathrm{F}(\theta,\phi) = -1\,, \tag{52}$$

and the traceless anti-involution Hermitian matrix

$$\mathrm{s}(\phi) = \begin{pmatrix} 0 & -\mathrm{e}^{-\mathrm{i}\phi} \\ \mathrm{e}^{\mathrm{i}\phi} & 0 \end{pmatrix}, \quad \mathrm{s}^2 = -\mathbb{1}_2\,, \quad \det \mathrm{s}(\phi) = 1 \tag{53}$$

are introduced.

Note the relations preserving the traceless property:

$$\mathrm{s}(\phi)\,\mathrm{F}(\theta,\phi) = \begin{pmatrix} -\cos\frac{\theta}{2} & -\sin\frac{\theta}{2}\mathrm{e}^{-\mathrm{i}\phi} \\ -\sin\frac{\theta}{2}\mathrm{e}^{\mathrm{i}\phi} & \cos\frac{\theta}{2} \end{pmatrix} = \mathrm{F}(\theta+\pi,\phi) = -\mathrm{F}(\theta,\phi)\,\mathrm{s}(\phi)\,, \tag{54}$$

and also note that the traceless features on both sides of Equation (51) are respected.

Let us now calculate the commutator $\left[\dot{U}U^\dagger, \sigma_{\theta,\phi}\right]$ on the left-hand side of Equation (49). From the relations

$$\mathrm{F}(\theta,\phi)\,\sigma_{\theta,\phi} = U(\pi-\theta,\phi)\,, \quad \sigma_{\theta,\phi}\,\mathrm{F}(\theta,\phi) = U^\dagger(\pi-\theta,\phi)\,, \tag{55}$$

$$\mathrm{s}(\phi)\,\sigma_{\theta,\phi} = \sigma_{\theta+\frac{\pi}{2},\phi} = -\sigma_{\theta,\phi}\,\mathrm{s}(\phi) \Leftrightarrow \sigma_{\theta,\phi}\,\sigma_{\theta+\frac{\pi}{2},\phi} = -\mathrm{s}(\phi) = -\sigma_{\theta+\frac{\pi}{2},\phi}\,\sigma_{\theta,\phi}\,, \tag{56}$$

one obtains

$$\left[\dot{U}U^\dagger, \sigma_{\theta,\phi}\right] = \mathrm{i}\dot{\phi}\,\sin\theta\,\mathrm{s}(\phi) + \dot{\theta}\,\sigma_{\theta+\frac{\pi}{2},\phi} \tag{57}$$

and

$$\left[\dot{U}U^\dagger, \sigma_{\theta,\phi}\right]\sigma_{\theta,\phi} = \mathrm{i}\dot{\phi}\,\sin\theta\,\sigma_{\theta+\frac{\pi}{2},\phi} + \dot{\theta}\,\mathrm{s}(\phi)\,. \tag{58}$$

The set of properties (57) and (58) allow obtaining separate equations for the angular variables. Starting from Equation (47), we write

$$\left[\dot{U}U^\dagger, \sigma_{\theta,\phi}\right]\sigma_{\theta,\phi} = \mathrm{i}\dot{\phi}\,\sin\theta\,\sigma_{\theta+\frac{\pi}{2},\phi} + \dot{\theta}\,\mathrm{s}(\phi) = N(\theta,\phi)\,, \tag{59}$$

and then multiplying each term of Equation (59) by $\sigma_{\theta+\frac{\pi}{2},\phi}$ and tracing the result yield

$$\begin{aligned} 2\mathrm{i}\dot{\phi}\,\sin\theta &= \mathrm{Tr}\left[N(\theta,\phi)\,\sigma_{\theta+\frac{\pi}{2},\phi}\right] \\ &= 2\mathrm{i}[\sin\theta\,(h_{00}-h_{11}) - 2\cos\theta\,(\mathrm{Re}\,h_{01}\,\cos\phi - \mathrm{Im}\,h_{01}\,\sin\phi) + (h_2-h_1)\sin\theta\,\sin 2\phi]\,, \end{aligned} \tag{60}$$

where the h_{ij} are the matrix elements of H, $H = \begin{pmatrix} h_{00} & h_{01} \\ \overline{h_{01}} & h_{11} \end{pmatrix}$, where $\overline{h_{01}}$ is the conjugate of h_{01}. After simplification, for $\theta \neq 0, \pi$,

$$\dot{\phi} = h_{00} - h_{11} - 2\cot\theta\,(\mathrm{Re}\,h_{01}\,\cos\phi - \mathrm{Im}\,h_{01}\,\sin\phi) + (h_2-h_1)\,\sin 2\phi\,. \tag{61}$$

Similarly, multiplying Equation (51) by $\mathrm{s}(\phi)$, tracing the result, and dividing by two yield

$$\dot{\theta} = -2(\mathrm{Re}\,h_{01}\,\sin\phi + \mathrm{Im}\,h_{01}\,\cos\phi) + \sin 2\theta(h_1\cos^2\phi + h_2\sin^2\phi - h_3)\,. \tag{62}$$

The Ricatti-like Equations (61) and (62) can be interpreted as the equations of motion for the orientation of the Bloch vector on the sphere. They demonstrate how both the Hamiltonian and the decay rates contribute to the rotation and evolution of the quantum state's direction. The Hamiltonian terms h_{ij} drive the coherent precession, while the decay rates h_k induce a drift or move toward a new non-rotational final position. The final state of the system is a balance between these two competing effects.

3.2.3. The Full Dynamical System

Combining the evolution equations for angular (61)–(62) and radial (43) variables one finally obtains the system

$$\dot{\phi} = h_{00} - h_{11} - 2\cot\theta\,(\mathrm{Re}\,h_{01}\,\cos\phi - \mathrm{Im}\,h_{01}\,\sin\phi) + (h_2-h_1)\,\sin 2\phi\,, \tag{63}$$

$$\dot{\theta} = -2(\mathrm{Re}\,h_{01}\,\sin\phi + \mathrm{Im}\,h_{01}\,\cos\phi) + \sin 2\theta(h_1\cos^2\phi + h_2\sin^2\phi - h_3)\,, \tag{64}$$

$$\frac{\dot{r}}{r} = -2\left[h_1(1-\sin^2\theta\cos^2\phi) + h_2(1-\sin^2\theta\sin^2\phi) + h_3\sin^2\theta\right]. \tag{65}$$

As a natural example, for the particular cases where H is diagonal and time-independent, h_1, h_2, h_3 with $h_1 = h_2$, one obtains the solution

$$\phi(t) = \phi_0 + (h_{00} - h_{11})(t - t_0)\,, \tag{66}$$

$$\tan\theta(t) = \tan\theta_0\, \mathrm{e}^{-2(h_3 - h_1)t}\,, \tag{67}$$

$$r(t) = r_0\, \mathrm{e}^{-4h_1 t}\, |\cos\theta_0| \sqrt{1 + \tan^2\theta_0\, \mathrm{e}^{-4(h_3 - h_1)t}} \tag{68}$$

to Equations (63)–(65), respectively.

Note the invariant trajectories which are derived from Equations (67) and (68):

$$r(t)\,|\cos\theta(t)|\,|\tan\theta(t)|^{-2h_1/(h_3 - h_1)} = r_0\,|\cos\theta_0|\,|\tan\theta_0|^{-2h_1/(h_3 - h_1)} \quad (h_3 - h_1 \neq 0)\,. \tag{69}$$

Equation (69) is a geometric constraints equation that defines the exact shape of the spiral inside the Bloch ball. Solution (27) corresponds to the particular choices $h_1 = 0$, $h_3 = h$, $t_0 = 0$, $\phi_0 = 0$, $h_{00} - h_{11} = 2\omega_0$, $r_0 = 1$, and $\theta_0 = \pi/4$.

4. Fixed Points: Discussion

The asymptotic behavior of an open quantum system is characterized by its set of stationary or fixed points. As already presented in Section 2.4, the z-axis of the Bloch ball represents a set of fixed points. This corresponds to $h_1 = h_2 = 0$, $\theta_0 = 0$, and $e_1 = e_2 = 0$ (in Equation (3)) or $\mathrm{Re}\, h_{01} = \mathrm{Im}\, h_{01} = 0$ (in Equation (64)). The other two axes (x and y) of the Bloch ball are also sets of fixed points, and this case corresponds to the values of parameters $e_2 = e_3 = h_2 = h_3 = 0$ for the x-axis ($\phi_0 = 0$, $\theta_0 = \pi/2$) and $e_1 = e_3 = h_1 = h_3 = 0$ for the y-axis ($\phi_0 = \pi/2$, $\theta_0 = \pi/2$). This can be verified by substituting those values into Equations (63)–(65).

The fixed points of the system, denoted by $\vec{a}_*$, are identified by solving the steady-state condition $\dot{\vec{a}} = 0$ for the governing dynamics in Equation (5). Once the fixed points are determined, their stability is ascertained through linear stability analysis. This procedure involves analyzing the evolution of an infinitesimal perturbation, $\vec{\delta}$, from a fixed point, such that $\vec{a}(t) = \vec{a}_* + \vec{\delta}(t)$. Substituting this into the equations for the system and retaining only first-order terms in $\vec{\delta}$ yield a set of linear differential equations describing the dynamics of the perturbation. The stability of the fixed point is then determined by the eigenvalues of the corresponding Jacobian matrix.

To illustrate this methodology, we apply it to the system presented in Section 2.4 whose dynamics are given by Equation (4). The linearization around a fixed point $\vec{a}_*$ results in a system for the perturbation $\vec{\delta}$. By the definition of a fixed point, the static terms vanish, yielding the following linear system:

$$\dot{\vec{\delta}} = -2 \begin{pmatrix} h & \omega_0 & 0 \\ -\omega_0 & h & 0 \\ 0 & 0 & 0 \end{pmatrix} \vec{\delta}\,. \tag{70}$$

The eigenvalues of the Jacobian matrix are readily found to be $\lambda_1 = -2h - 2i\omega_0$, $\lambda_2 = -2h + 2i\omega_0$, and $\lambda_3 = 0$.

Since $h > 0$, the real parts of the complex conjugate eigenvalues $\lambda_{1,2}$ are negative. This implies that the dynamics are asymptotically stable in the $a_1 a_2$-plane. Any perturbation in this plane decays, returning the system to the fixed point. Conversely, the null eigenvalue, $\lambda_3 = 0$, indicates neutral stability along the a_3 direction. This signifies the existence of a continuum of equilibrium points. Collectively, these results demonstrate that the system possesses a line of fixed points, where each point on this line is an attractor for the dynamics

within its respective a_1a_2-plane (i.e., for a constant a_3). Since the system under consideration is linear, this stability analysis is exact and provides a complete characterization of the equilibrium structure.

It is known [19] that the existence of multiple steady states is fundamentally linked to the presence of symmetries or a decomposable structure in the dynamics of the system. A system is considered decomposable if its Hilbert space can be broken down into two or more orthogonal subspaces that are invariant under the evolution. If such subspaces exist, the system cannot have a single globally attractive fixed point.

The study of fixed points and steady states is related to reservoir engineering [20]. By attentively designing a qubit's Hamiltonian and its dissipative interactions with an environment, one can control the final steady state that the system evolves toward. This is a powerful tool for both state preparation, where a qubit is forced into a desired pure or mixed state, and for stabilization. In the latter case, the dissipative process actively protects a specific quantum state from noise by providing a form of continuous error correction, always pulling the state back toward the stable fixed point. Then, if the dynamics allows for multiple stable fixed points, this collection of states can be used as a robust memory. Each distinct fixed point can encode a piece of information, and the stability of these points makes the memory fault-tolerant or self-correcting, as the system's natural evolution resists perturbations that may alter the stored information.

5. Conclusions

In this paper, we have examined two complementary approaches to the GKSL equation for an open qubit. The first approach, essentially being the standard method, exploits the linear structure of the equation and enables the systematic construction of explicit solutions; we illustrated this approach by analyzing representative trajectories within the Bloch ball.

The second approach leverages the underlying $\mathrm{SU}(2)$ symmetry of the Bloch ball and recasts the problem as a nonlinear dynamical system, thereby provides a geometrically motivated alternative description of the same open-system dynamics.

Although more intricate, this second formulation highlights in a natural way the distinction between the angular dynamics of the system and the radial component associated with dissipation. The main appeal of this second perspective lies in its potential for generalization to the GKSL equation for open qudits, i.e., higher-dimensional generalizations of qubits.

Along these lines, the $\mathrm{SU}(2)$–symmetry approach allows a natural generalization by invoking the coset symmetry $\mathrm{SU}(N)/\mathrm{U}(1)^{N-1}$ together with a corresponding generalized angular-coordinate parametrization. This extension is justified, since for an arbitrary N-level system (qudit), the Lie algebra $\mathfrak{su}(N)$ possesses $N-1$ independent Casimir invariants, which may be associated with a set of $N-1$ "radial" variables. As a consequence, one can partially decouple the dynamics of the GKSL equation: the evolution separates into contributions controlling the state's purity, the decay rates along the different Casimir directions, and the nonlinear dynamics governing the orientation of the generalized Bloch vector on the coset manifold. This provides a geometric framework in which dissipation and rotation are quite well distinguished on the level of the dynamical system.

On the other hand, the linear analysis provided direct physical understanding, as illustrated by the case where dissipation affects only the xy-plane components, revealing a line of stable fixed points along the z-axis that acts as an attractor for the quantum states. These lines (the three axes) of stable fixed points may be employed to protect quantum information by engineering the right qubit–environment interactions.

Author Contributions: Conceptualization, A.C.M., E.M.F.C., J.-P.G. and T.K.; methodology, A.C.M., E.M.F.C., J.-P.G. and T.K.; software, A.C.M., E.M.F.C., J.-P.G. and T.K.; validation, A.C.M., E.M.F.C., J.-P.G. and T.K.; formal analysis, A.C.M., E.M.F.C., J.-P.G. and T.K.; investigation, A.C.M., E.M.F.C., J.-P.G. and T.K.; resources, A.C.M., E.M.F.C., J.-P.G. and T.K.; data curation, A.C.M., E.M.F.C., J.-P.G. and T.K.; writing—original draft preparation, A.C.M., E.M.F.C., J.-P.G. and T.K.; writing—review and editing, A.C.M., E.M.F.C., J.-P.G. and T.K.; visualization, A.C.M., E.M.F.C., J.-P.G. and T.K.; supervision, A.C.M., E.M.F.C., J.-P.G. and T.K.; project administration, A.C.M., E.M.F.C., J.-P.G. and T.K.; funding acquisition, A.C.M., E.M.F.C., J.-P.G. and T.K. All authors have read and agreed to the published version of the manuscript.

Funding: We thank for the financial support the Brazilian scientific agencies Fundação de Amparo à Pesquisa do Estado do Rio de Janeiro (FAPERJ), Coordenação de Aperfeiçoamento de Pessoal de Nível Superior (CAPES), and Conselho Nacional de Desenvolvimento Científico e Tecnológico (CNPq). T.K. acknowledges the financial support by CNPq (No. 305654/2021-7; 304504/2024-6). A part of this work has been done under the project INCT-Nuclear Physics and Applications (No. 464898/2014-5).

Data Availability Statement: No new data were created or analyzed in this study.

Acknowledgments: During the preparation of this manuscript, the authors used *ChatGPT* (OpenAI, GPT-4–class models, accessed during 2024–2025) and *Gemini* (Google DeepMind, Gemini 1.x models, accessed during 2024–2025) for the purpose of language editing and writing assistance. The authors have reviewed and edited all AI-generated content and take full responsibility for the content of this publication. E.M.F.C. acknowledges the Conselho Nacional de Desenvolvimento Científico e Tecnológico (CNPq) and the Fundação de Amparo à Pesquisa do Estado do Rio de Janeiro (FAPERJ), Brazil.

Conflicts of Interest: The authors declare no conflicts of interest. The funders had no role in the design of the study; in the collection, analyses, or interpretation of data; in the writing of the manuscript; or in the decision to publish the results.

Appendix A. Behavior for Long Times

For the sake of clarity, we keep the expression $\sqrt{\beta^2-1}$ here instead of using $\widetilde{\gamma}$. Following the example related to Equation (22), we can substitute the hyperbolic trigonometric functions by their exponential counterparts

$$\vec{a}(t) = e^{-ht}\left(\left[\frac{e^{(2\omega_0 t\sqrt{\beta^2-1})}+e^{-(2\omega_0 t\sqrt{\beta^2-1})}}{2}+\frac{\beta\left(e^{(2\omega_0 t\sqrt{\beta^2-1})}-e^{-(2\omega_0 t\sqrt{\beta^2-1})}\right)}{2\sqrt{\beta^2-1}}\right], \quad \text{(A1)}$$

$$\frac{e^{(2\omega_0 t\sqrt{\beta^2-1})}-e^{-(2\omega_0 t\sqrt{\beta^2-1})}}{2\sqrt{\beta^2-1}}, 0\Bigg)^{\mathrm{T}}, \quad \text{(A2)}$$

so that then, there are two exponentials with arguments $-t(h+2\omega_0\sqrt{\beta^2-1})$ and $-t(h-2\omega_0\sqrt{\beta^2-1})$, where the former argument describes faster decay than the latter argument. So, for a long enough time

$$e^{-ht-2\omega_0 t\sqrt{\beta^2-1}} \to 0, \quad \text{(A3)}$$

and the system asymptotically behaves as

$$\vec{a}(t) \to \left(\left[\frac{e^{-ht+2\omega_0 t\sqrt{\beta^2-1}}}{2}+\frac{\beta e^{-ht+2\omega_0 t\sqrt{\beta^2-1}}}{2\sqrt{\beta^2-1}}\right], \frac{e^{-ht+2\omega_0 t\sqrt{\beta^2-1}}}{2\sqrt{\beta^2-1}}, 0\right)^{\mathrm{T}}. \quad \text{(A4)}$$

Then,

$$\tau_d = \frac{1}{h-2\omega_0\sqrt{\beta^2-1}}, \quad \text{(A5)}$$

can be defined and, after some manipulations, Equation (A4) transforms to Equation (24). Thus, factoring out the exponentials, the norm is

$$\|\vec{a}(t)\| \to \mathrm{e}^{-t/\tau_d}\left(\frac{\beta^2+\beta\sqrt{\beta^2-1}}{\sqrt{\beta^2-1}}\right)^{1/2} = \mathrm{e}^{-t/\tau_d}\left(\frac{2\omega_0\tau_d\beta}{\sqrt{\beta^2-1}}\right)^{1/2}. \tag{A6}$$

Therefore, for times as long as $t \gg \tau_d$,

$$\|\vec{a}(t)\| \propto \mathrm{e}^{-t/\tau_d}. \tag{A7}$$

Appendix B. One Qbit Dynamic System

The GKSL Equation (1) with density operators

$$\frac{\mathrm{d}\rho}{\mathrm{d}t} = \mathrm{i}\,[H,\rho] + \sum_{k=1}^{3} h_k[\sigma_k\rho\sigma_k - \rho]\,, \tag{A8}$$

where the jump operators like the Pauli matrices substituted L_k become straightforwardly solvable by writing the density matrix with Einstein's notation:.

$$\rho = \frac{1}{2}(\mathbb{1}_2 + a_1\sigma_1 + a_2\sigma_2 + a_3\sigma_3) \equiv \frac{1}{2}\left(\mathbb{1}_2 + a_j\sigma_j\right), \tag{A9}$$

and analogously, the Hamiltonian becomes

$$H = e_0\mathbb{1}_2 + e_\mu\sigma_\mu\,, \tag{A10}$$

with $j,\mu = 1,2$, and 3. Then, the commutator of Equation (A8) is written as

$$\mathrm{i}[H,\rho] = \frac{\mathrm{i}}{2}\left[\left(e_0\mathbb{1}_2 + e_\mu\sigma_\mu\right)\left(\mathbb{1}_2 + a_j\sigma_j\right) - \left(\mathbb{1}_2 + a_j\sigma_j\right)\left(e_0\mathbb{1}_2 + e_\mu\sigma_\mu\right)\right], \tag{A11}$$

$$= \frac{\mathrm{i}}{2}\left[e_\mu\sigma_\mu a_j\sigma_j - a_j\sigma_j e_\mu\sigma_\mu\right], \tag{A12}$$

$$= \frac{\mathrm{i}e_\mu a_j}{2}\left(\mathrm{i}\epsilon_{\mu jl} - \mathrm{i}\epsilon_{j\mu l}\right) = -e_\mu a_j\epsilon_{\mu jl}\sigma_l\,, \tag{A13}$$

with $\epsilon_{\mu jl}$ the Levi-Civita symbol, while the derivative

$$\frac{\mathrm{d}\rho}{\mathrm{d}t} = \frac{\dot{a}_m}{2}\sigma_m\,. \tag{A14}$$

Before determining directly the sum in Equation (A8), it is worthy to state that any matrix of order two can be written in terms of the identity and the Pauli matrices, for example, matrix M

$$M = m_0\mathbb{1}_2 + m_1\sigma_1 + m_2\sigma_2 + m_3\sigma_3, \tag{A15}$$

where the coefficients m_0, m_n are obtained via

$$m_0 = \frac{1}{2}\mathrm{Tr}[M], \tag{A16}$$

$$m_n = \frac{1}{2}\mathrm{Tr}[\sigma_n M]\,. \tag{A17}$$

Thus, the coefficients of the left-hand side of Equation (A8) are extracted from Equation (A14):

$$\frac{1}{2}\mathrm{Tr}\left[\sigma_n\frac{\mathrm{d}\rho}{\mathrm{d}t}\right] = \frac{\dot{a}_n}{2}, \tag{A18}$$

and the n-th coefficient of the commutator in Equation (A13):

$$\frac{1}{2}\mathrm{Tr}[\sigma_n \, \mathrm{i}[H,\rho]\,] = -e_\mu a_j \epsilon_{\mu jn} \,. \tag{A19}$$

Now, the coefficients related to the sum of Equation (A8) are determined by

$$\frac{1}{2}\mathrm{Tr}\left[\sigma_n\left(\sum_k h_k\sigma_k\rho\sigma_k - h_k\rho\right)\right] = \sum_{k,l=1}^{3} h_k\left\{\frac{a_l}{4}\mathrm{Tr}[\sigma_n\sigma_k\sigma_l\sigma_k] - \frac{a_n}{2}\right\} \tag{A20}$$

and, with the help of the identity $\mathrm{Tr}\left[\sigma_i\sigma_j\sigma_k\sigma_l\right] = 2\Big(\delta_{ij}\delta_{kl} - \delta_{ik}\delta_{jl} + \delta_{il}\delta_{jk}\Big)$, Equation (A20), where δ_{ij} is the Kronecker delta, reads

$$\frac{1}{2}\mathrm{Tr}\left[\sigma_n\left(\sum_k h_k\sigma_k\rho\sigma_k - h_k\rho\right)\right] = h_n a_n - a_n\sum_{k=1}^{3} h_k \,. \tag{A21}$$

Therefore, the GKSL equation based on Equations (A18), (A19), and (A21) reads

$$\frac{\dot{a}_n}{2} = -e_\mu a_j \epsilon_{\mu jn} + a_n\left(h_n - \sum_{k=1}^{3} h_k\right), \tag{A22}$$

which represents the set in Equation (4).

References

1. Nielsen, M.A.; Chuang, I.L. *Quantum Computation and Quantum Information*; Cambridge University Press: New York, NY, USA, 2000. Available online: https://archive.org/details/quantumcomputati0000niel/ (accessed on 1 December 2025).
2. Breuer, H.-P.; Petruccione, F. *The Theory of Open Quantum Systems*; Oxford University Press Inc.: New York, NY, USA, 2007. [CrossRef]
3. Dodonov, A.V.; Mizrahi, S.S.; Dodonov, V.V. Microscopic models of quantum-jump superoperators. *Phys. Rev. A* **2005**, *72*, 023816. [CrossRef]
4. Alipour, S.; Mehboudi, M.; Rezakhani, A.T. Quantum metrology in open systems: Dissipative Cramér–Rao bound. *Phys. Rev. Lett.* **2014**, *112*, 120405. [CrossRef] [PubMed]
5. Jirari, H.; Putz, W. Optimal coherent control of dissipative N-level systems. *Phys. Rev. A* **2005**, *72*, 013409. [CrossRef]
6. Curado, E.M.F.; Faci, S.; Gazeau, J.-P.; Koide, T.; Maioli, A.C.; Noguera, D. Quantum circuit complexity for linearly polarized light. *Phys. Rev. A* **2025**, *111*, 032208. [CrossRef]
7. Rivas, Á.; Huelga, S.F. *Open Quantum Systems. An Introduction*; Springer: Berlin/Heidelberg, Germany, 2012. [CrossRef]
8. Daniel, M. A short introduction to the Lindblad master equation. *AIP Adv.* **2020**, *10*, 025106. [CrossRef]
9. Chruściński, D.; Pascazio, S. A brief history of the GKSL equation. *Open Syst. Inform. Dyn.* **2017**, *24*, 1740001. [CrossRef]
10. Salgado, D.; Sánchez-Gómez, J.L. A Formula for the Bloch vector of some Lindblad quantum systems. *J. Phys. A Math. Gen.* **2004**, *37*, 9507–9523. [CrossRef]
11. Klimov, A.B.; Chumakov, S.M. *A Group-Theoretical Approach to Quantum Optics: Models of Atom-Field Interactions*; Wiley-VCH Verlag GmbH & Co. KGaA: Weinheim, Germany, 2009. [CrossRef]
12. Verstraete, F.; Wolf, M.M.; Cirac, J.I. Quantum computation and quantum-state engineering driven by dissipation. *Nat. Phys.* **2009**, *5*, 633–636. [CrossRef]
13. Pastawski, F.; Clemente, L.; Cirac, J.I. Quantum memories based on engineered dissipation. *Phys. Rev. A* **2011**, *83*, 012304. [CrossRef]
14. Lidar, D.A.; Birgitta Whaley, K. Decoherence-free subspaces and subsystems. In *Irreversible Quantum Dynamics*; Benatti, F., Floreanini, R., Eds.; Springer: Berlin/Heidelberg, Germany, 2003; pp. 83–120.
15. Altafini, C.; Ticozzi, F. Modeling and control of quantum systems: An introduction. *IEEE Trans. Autom. Control* **2012**, *57*, 1898–1917. [CrossRef]
16. Heiss, W.D. Exceptional points of non-Hermitian operators. *J. Phys. A Math. Gen.* **2004**, *37*, 2455–2464. [CrossRef]
17. Miri, M.-A.; Alù, A. Exceptional points in optics and photonics. *Science* **2019**, *363*, eaar7709. [CrossRef] [PubMed]
18. Naghiloo, M.; Abbasi, M.; Joglekar, Y.N.; Murch, K.W. Quantum state tomography across the exceptional point in a single dissipative qubit. *Nat. Phys.* **2019**, *15*, 1232–1236. [CrossRef]

19. Schirmer, S.G.; Wang, X. Stabilizing open quantum systems by Markovian reservoir engineering. *Phys. Rev. A* **2009**, *81*, 062306.
20. Rakovszky, T.; Gopalakrishnan, S.; von Keyserlingk, C. Defining stable phases of open quantum systems. *Phys. Rev. X* **2024**, *14*, 041031. [CrossRef]